

Hamiltonian Benchmark of a Solid-State Spin-Photon Interface for Computation

Tejas Acharya,^{1,2,3,*} Loïc Lanço,^{4,5} Olivier Krebs,⁴ Hui Khoon Ng,^{1,2,3} Alexia Auffèves,^{2,3} and Maria Maffei^{6,†}

¹*Department of Physics, National University of Singapore, 117551 Singapore, Singapore*

²*Centre for Quantum Technologies, National University of Singapore, 117543 Singapore, Singapore*

³*MajuLab, CNRS-UCA-SU-NUS-NTU International Joint Research Laboratory*

⁴*Université Paris-Saclay, CNRS, Centre de Nanosciences et de Nanotechnologies, 91120 Palaiseau, France*

⁵*Université Paris Cité, Centre de Nanosciences et de Nanotechnologies, 91120 Palaiseau, France*

⁶*Université de Lorraine, CNRS, Laboratoire de Physique et Chimie Théoriques, 54500 Vandoeuvre-les-Nancy, France*

Light-matter interfaces are pivotal for quantum computation and communication with photons. At the fundamental level, they are interacting quantum systems made of an emitter and a propagating electromagnetic field. The interaction maps qubits encoded in the emitter's degrees of freedom — energy or spin — onto photonic degrees of freedom — polarization or photon-number — featuring flying qubits. In this way it is possible to design photon-photon gates or to produce photonic cluster states. Quantum interfaces' dynamics is often solved within the single-mode approximation or open quantum system approach. Such effective models imply losing information about multi-mode states of the propagating field, and about light-matter entanglement, often hindering the exact modeling of protocols. In this work, we solve the full Hamiltonian dynamics of a solid-state spin-photon interface for three protocols relevant for photon-based quantum computation: the generation of superpositions of photon-number states, a controlled photon-photon gate, and the production of photonic cluster states. We then derive the realistic performance of these schemes and display where their fundamental limitations lie. Our study reveals that realistic experimental imperfections severely limit the performance of the photon-photon gate, slightly affect the fidelity of linear photonic clusters, and are nearly harmless for the generation of photon-number superpositions.

I. INTRODUCTION

Light-matter interfaces are composite systems that feature quantum emitters in interaction with propagating electromagnetic fields. They are fundamental building blocks for quantum communication and distributed quantum computing allowing the mapping of stationary qubits, encoded in the emitters, onto flying qubits, encoded in photons [1]. Confining the field in one dimension maximizes the effectiveness of the light-matter coupling and hence the interface performance [2]. Spin-photon interfaces (SPIs) feature emitters with an internal spin degree of freedom. Due to conservation of angular momentum, transitions between states with different spin projections are coupled with different polarization modes of the electromagnetic field. Energy gaps can be tuned with magnetic fields, and selection rules can be harnessed to tailor specific field's states. Exploiting these mechanisms, SPIs can be used to implement controlled photon-photon gates [3, 4] or clusters of entangled photons [5–7].

Experimental implementations of SPIs range from atomic physics [8–10], ion traps [11], to solid-state semiconductor devices [12–18]. This article focuses on the latter, inspired by recent experimental progress in this field [15–18]. We aim to reveal the mechanisms affecting the performance of solid-state SPIs under realistic conditions and to quantify their impact on relevant technological protocols. To this end, we analyze three protocols: the generation of arbitrary superpositions of photon-number states [19, 20]; the controlled photon-photon gate proposed in [3]; and the generation of photonic clusters proposed in [5] and recently implemented in [15–17].

Our analysis is based on the Hamiltonian evolution of light-matter entangled wavefunctions and hence it does not involve any loss of information on the state of the propagating electromagnetic field nor on the spin-photon entanglement. This allows us to fill two gaps in the existing literature. First: pioneering proposals involving SPIs assumed monochromatic photons [3, 5, 6], yet propagating electromagnetic fields are infinite reservoirs of frequency modes and flying photonic qubits correspond to wavepackets of finite bandwidths. The multi-mode nature of propagating fields introduces an intrinsic decoherence mechanism that one must consider in order to exactly characterize the protocols. Second, in realistic solid-state SPIs the spin suffers from additional decoherence due to the charge dynamics and its hyperfine interaction with the nuclear spins of the atoms forming the device [21]. This effect has been neglected in most theoretical proposals and included in experimental analyses only as an effective dephasing term in the spin open evolution. Our model includes the spin hyperfine interaction in the light-matter Hamiltonian and yields spin decoherence after classical averaging over many microscopic configurations. Our results reveal the impact of the different decoherence mechanisms and display how they conspire to lower the fidelity of the considered protocols.

II. SYSTEM AND MODEL

The SPI is implemented with a quantum dot charged with an extra electron spin and embedded in a semi-transparent micro-cavity which provides a highly efficient coupling to the electromagnetic field on one side of the emitter. This structure gives rise to a nearly perfect confinement of the field in one semi-axis, a geometry often called "half 1D", see Fig. (1a). All along the paper, we consider that the SPI is kept at a cryo-

* tejas.acharya@u.nus.edu

† maria.maffei1@gmail.com

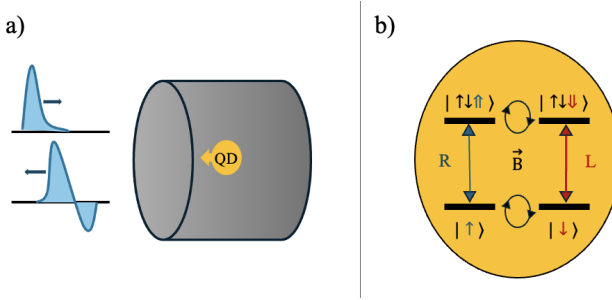


Figure 1: Spin-photon interface implemented with a charged quantum dot (QD) in a directional micro-cavity, schematics.

a) The directional micro-cavity confines the field to propagate along half of the z axis, i.e. input and output fields travel on the same side of the emitter. b) Structure of the energy levels of the charged QD: a degenerate 4-level system with optical selection rules, R and L stand for right- and left-circular polarization respectively.

genic temperature and hence is immune to phonon-induced decoherence [19, 20].

In the absence of an applied magnetic field, the charged QD can be modeled as a degenerate 4-level emitter: two ground states, belonging to the trapped electron, $\{|\uparrow\downarrow\rangle, |\downarrow\uparrow\rangle\}$, with spin projections $\pm 1/2$ along the quantization axis, z , defined by the growth direction of the QD and the propagation of the electromagnetic field; and two excited states, belonging to an optically excited spin-hole pair, or trion, $\{|\uparrow\downarrow\uparrow\rangle, |\uparrow\downarrow\downarrow\rangle\}$, with spin projections along z being $\pm 3/2$. Then the bare Hamiltonian of the QD reads $H_{QD} = \hbar\omega_0(|\uparrow\downarrow\uparrow\rangle\langle\uparrow\downarrow\uparrow| + |\uparrow\downarrow\downarrow\rangle\langle\uparrow\downarrow\downarrow|)$. Conservation of the angular momentum gives rise to optical selection rules: the transition $|\downarrow\rangle \rightarrow |\uparrow\downarrow\downarrow\rangle$ (resp. $|\uparrow\rangle \rightarrow |\uparrow\downarrow\uparrow\rangle$) can only be promoted by absorption of a left- (resp. right-) circularly polarized photon, see Fig. (1b).

The propagating field is described as a continuous reservoir of modes of frequency ω and wavenumber k verifying a linear dispersion relation around the emitter's frequency ω_0 , $(k-k_0) = (\omega-\omega_0)/v_g$, with v_g being its group velocity. Adopting the standard treatment for half 1D geometries, we consider only positive values of k and v_g and unfold the z axis around the emitter's position ($z=0$) hence mapping backwards propagation in the negative semi-axis onto forwards propagation in the positive semi-axis. Then, the field's bare Hamiltonian reads $H_f = \hbar \int d\omega \omega [a_R^\dagger(\omega)a_R(\omega) + a_L^\dagger(\omega)a_L(\omega)]$, where L and R stand for left- and right-circularly polarized photons respectively, and $a_{L/R}(\omega)$ are annihilation operators verifying $[a_j(\omega), a_i^\dagger(\omega')] = \delta_{i,j}\delta(\omega - \omega')$ with $i, j \in \{L, R\}$. Assuming rotating-wave and flat coupling approximations, the interaction of the QD with the propagating field can be written as $V = i\hbar \int d\omega \sqrt{\gamma/(2\pi)} (|\downarrow\rangle\langle\uparrow\downarrow\downarrow| \otimes a_L^\dagger(\omega) + |\uparrow\rangle\langle\uparrow\downarrow\uparrow| \otimes a_R^\dagger(\omega)) - h.c.$, [22]. In this regime, we can define quantum noise operators destroying photons in the position z at time t : $b_{R(L)}(t, z) = (2\pi)^{-1/2} \int d\omega e^{-i(\omega-\omega_0)(t-z/vg)} a_{R(L)}(\omega) = b_{R(L)}(t - z/vg, 0)$, with $[b_i(t, 0), b_j^\dagger(t', 0)] = \delta_{i,j}\delta(t - t')$ [23]. The QD is positioned in $z = 0$, so, from now on we will set $b_j(t, 0) \equiv b_j(t)$ to shorten the notation. Then, in the interaction picture with respect to

$H_{QD} + H_f$, the light-matter coupling becomes

$$V_I(t) = i\hbar \sqrt{\gamma} (|\downarrow\rangle\langle\uparrow\downarrow\downarrow| \otimes b_L^\dagger(t) + |\uparrow\rangle\langle\uparrow\downarrow\uparrow| \otimes b_R^\dagger(t)) - h.c. \quad (1)$$

Magnetic Hamiltonian

In a realistic QD at low temperatures the spin undergoes two kinds of dynamics: a coherent precession induced by an external magnetic field, and a decoherence process due to the interaction with the surrounding nuclei. Here we consider only the so-called Voigt configuration where the external magnetic field is perpendicular to the spin quantization axis, z . A complete description should consider that the trion Landé factor is a tensor, such that the magnetic Hamiltonian of the trion spin would depend on the magnetic field orientation [24]. However, here we consider a simplified, yet accurate enough, model in which the trion Landé factor is isotropic in the (x, y) plane leading to an effectively scalar and positive Landé factor g_{tr} . As recently shown in [25], this condition can be attained experimentally via fine tuning of the angle between the polarization of the light pulse used to excite the trion and the direction of the magnetic field. In the rest of the paper, for simplicity, we will take the latter to be coincident with the x axis. The magnetic field then reads $\mathbf{B}^{ext} = B^{ext}\hat{x}$ and the magnetic Hamiltonian reads $H_s^{ext} = \mu_B B^{ext} [g_{tr}s_x^{tr} + g_{el}s_x^{el}]/2$ where μ_B is the Bohr magneton, g_{tr} and g_{el} are trion and electron Landé factors, and $s_x^{tr(el)} \equiv s^{tr(el)} + (s^{tr(el)})^\dagger$ are their x Pauli matrices, with $s^{tr} = |\uparrow\downarrow\downarrow\rangle\langle\uparrow\downarrow\downarrow|$ and $s^{el} = |\downarrow\rangle\langle\uparrow\downarrow|$.

At low temperatures, the main incoherent contribution to the spin dynamics comes from the hyperfine interaction of the electron spin with the nuclear spins of the $\sim 10^5$ atoms that compose the nanostructure, this interaction can be modeled as an effective magnetic field, called Overhauser field, \mathbf{B}^O , around which the electron spin effectively precesses [21]. Let us notice that also the trion spin is effectively coupled with an Overhauser field, but since the latter is one order of magnitude smaller we neglect it. The intensity of the (electron) Overhauser field is of the order of tens of mT and its direction fluctuates as result of the changing nuclear environment. The most important semi-classical model to describe the electron spin decoherence in semiconductor QDs is given by the Merkulov-Efros-Rosen model [26], in which three distinct stages are described, each with its own characteristic timescale. In the first stage, or *frozen-nuclear-spin stage*, of the duration of a few hundred nanoseconds, the Overhauser field is considered static so that the electron spin coherently precesses around it. The statistical averaging over all possible intensities and orientations of the Overhauser field leads to a reduction of the average electronic spin polarization by a factor of 1/3 with respect to its initial value. The model then predicts a second stage where the Overhauser field is no longer static leading to a further reduction by a factor 1/3, until complete relaxation occurs after a few hundred microseconds [27]. In this paper, we study dynamics taking place on time-scales of a few hundred of nanoseconds meaning within the first stage of the relaxation process. This means that we

consider the Overhauser field frozen in a certain configuration and we add its coupling with the electron spin to the magnetic Hamiltonian of the external field:

$$H_s = H_s^{\text{ext}} + \frac{\mu_B g_{\text{el}}}{2} \mathbf{B}^O \cdot \mathbf{s}^{\text{el}} \equiv \frac{\hbar}{2} \left(\Omega_g \mathbf{n} \cdot \mathbf{s}^{\text{el}} + \Omega_e s_x^{\text{tr}} \right) \quad (2)$$

where we set $\hbar \Omega_e = g_{\text{tr}} \mu_B B^{\text{ext}}$ and $\hbar \Omega_g \mathbf{n} = g_{\text{el}} \mu_B (\mathbf{B}^O + \mathbf{B}^{\text{ext}})$ with $\mathbf{n} = (\sin(\theta) \cos(\phi); \sin(\theta) \sin(\phi); \cos(\theta))$ being a unit vector and $\mathbf{s}^{\text{el}} = (s_x^{\text{el}}; s_y^{\text{el}}; s_z^{\text{el}})$ being the vector of spin Pauli matrices for the electron spin. The expectation values of the observables are then computed by taking first quantum mechanical averages on pure states, corresponding to fixed Overhauser field configurations, and then classical averaging over all possible configurations. The latter are performed by using an isotropic Gaussian distribution centered around zero and having standard deviation w equal to the inverse relaxation time of the spin in the frozen-nuclear-spin stage. So, for instance the expectation value of the electron spin polarization s_z^{el} in the absence of external magnetic field, i.e. $\Omega_e = 0$ and $\Omega_g = \Omega_O = g_{\text{el}} \mu_B |\mathbf{B}^O|/\hbar$, starting from the electron spin state $|\uparrow\rangle$, is obtained from the statistical average of $\langle s_z^{\text{el}} \rangle = \cos^2\left(\frac{\Omega_O t}{2}\right) + \sin^2\left(\frac{\Omega_O t}{2}\right) \cos(2\theta)$:

$$\begin{aligned} \overline{s_z^{\text{el}}} &= \frac{\int_0^\infty \Omega_O^2 d\Omega_O \int_0^\pi \sin(\theta) d\theta \int_0^{2\pi} d\phi e^{-\Omega_O^2/2w^2} \langle s_z^{\text{el}} \rangle}{(2\pi w^2)^{3/2}} \quad (3) \\ &= \frac{1}{3} \left(1 + 2e^{-w^2 t^2/2} (1 - t^2 w^2) \right), \end{aligned}$$

which, in perfect agreement with the semi-classical prediction [26], reduces to $1/3$ for $t \gg w^{-1}$. In the rest of the paper, we use the notation \bar{X} to denote statistical averages of quantum mechanical expectation values that in turn will be denoted as $\langle X \rangle$.

A. Collision model of the SPI dynamics

Let us introduce a new notation that will help us simplify the calculations by decoupling the energy and the spin degrees of freedom. The basis of the SPI energy levels gets transformed as: $\{|\uparrow\rangle, |\downarrow\rangle\} \rightarrow \{|\uparrow\rangle|g\rangle, |\downarrow\rangle|g\rangle\}$ and $\{|\uparrow\downarrow\rangle, |\downarrow\uparrow\rangle\} \rightarrow \{|\uparrow\rangle|e\rangle, |\downarrow\rangle|e\rangle\}$. In the new basis, we define ladder operators acting on spin and energy degrees of freedom: $s \equiv |\downarrow\rangle\langle\uparrow|, \sigma \equiv |g\rangle\langle e|, s_z \equiv |\uparrow\rangle\langle\uparrow| - |\downarrow\rangle\langle\downarrow|$, and $\sigma_z \equiv |e\rangle\langle e| - |g\rangle\langle g|$. We will dub this notation "decoupled notation", and we will use it in all the equations from now on, unless explicitly stated otherwise. In the decoupled notation, omitting all identity operators, the terms of the Hamiltonian read: $H_{\text{QD}} = \hbar\omega_0 \sigma^\dagger \sigma$; $V_I(t) = i\hbar \sqrt{\gamma} (ss^\dagger \otimes \sigma \otimes b_L^\dagger(t) + s^\dagger s \otimes \sigma \otimes b_R^\dagger(t)) - h.c.$; and $H_s = \hbar/2 (\Omega_g \mathbf{n} \cdot \mathbf{s} \otimes \sigma \sigma^\dagger + \Omega_e s_x \otimes \sigma^\dagger \sigma)$.

We are now ready to find analytical expressions of the SPI wavefunction at any time during the dynamics using a collision model approach as in Refs. [28–31]. We take a coarse-graining time $\Delta t \ll \gamma^{-1}$, and define quantum noise increment operators $b_{j,n} \equiv (\Delta t)^{-1/2} \int_{n\Delta t}^{(n+1)\Delta t} dt b_j(t)$ with

$j = R, L$ and $[b_{i,n}, b_{j,m}^\dagger] = \delta_{i,j} \delta_{n,m}$. The operator $b_{R(L),n}$ destroys excitations in the n -th time-bin mode, or collision unit, of the right(left)-circularly polarized field that now is regarded as a sequence of units passing by the emitter's position on a conveyor belt. Using the commutation relations of the operators $b_{j,n}$ at different n , the unitary evolution operator evolving the joint light-matter system during the time interval $[n\Delta t, (n+1)\Delta t]$ can be written explicitly in the exponential form:

$$U_n = \exp \left\{ -\frac{i}{\hbar} \Delta t (H_s + V_n) \right\} \quad (4)$$

with

$$\begin{aligned} V_n &\equiv \frac{1}{\Delta t} \int_{n\Delta t}^{(n+1)\Delta t} dt' V_I(t') \\ &= \hbar i \sqrt{\frac{\gamma}{\Delta t}} (ss^\dagger \otimes \sigma \otimes b_{L,n}^\dagger + s^\dagger s \otimes \sigma \otimes b_{R,n}^\dagger) - h.c. \end{aligned} \quad (5)$$

It follows that the evolution until any time t can be decomposed in a product of $M = t/\Delta t$ independent collisions, i.e. $|\Psi(t)\rangle = \lim_{\Delta t \rightarrow 0} \prod_{n=0}^{M-1} U_n |\Psi(0)\rangle$. Writing the vacuum of the electromagnetic field in the basis of the collision units, $|0_R, 0_L\rangle = \bigotimes_n |0_{R,n}, 0_{L,n}\rangle$, with $b_{j,n} |0_{j,n}\rangle = 0$ and $b_{j,n}^\dagger |0_{j,n}\rangle = |1_{j,n}\rangle$, and expanding U_n up to the first order in $\gamma \Delta t$, one finds compact expressions for the emitter's Kraus operators corresponding to its no-jump evolution:

$$\begin{aligned} \mathcal{K}(t) &\equiv \lim_{\Delta t \rightarrow 0} \left(\prod_{n=0}^{t/\Delta t} \langle 0_{R,n}, 0_{L,n} | U_n | 0_{R,n}, 0_{L,n} \rangle \right) \quad (6) \\ &= e^{-i\frac{\Omega_O t}{2} \mathbf{n} \cdot \mathbf{s}} \otimes \sigma \sigma^\dagger + e^{-\gamma t/2} e^{-i\frac{\Omega_O t}{2} s_x} \otimes \sigma^\dagger \sigma, \end{aligned}$$

to its jump operators:

$$\begin{aligned} \mathcal{J}_R^{(-)} &\equiv \lim_{\Delta t \rightarrow 0} \frac{\langle 1_{R,n}, 0_{L,n} | U_n | 0_{R,n}, 0_{L,n} \rangle}{\sqrt{\Delta t}} = \sqrt{\gamma} s^\dagger s \otimes \sigma, \quad (7) \\ \mathcal{J}_L^{(-)} &\equiv \lim_{\Delta t \rightarrow 0} \frac{\langle 0_{R,n}, 1_{L,n} | U_n | 0_{R,n}, 0_{L,n} \rangle}{\sqrt{\Delta t}} = \sqrt{\gamma} s s^\dagger \otimes \sigma, \end{aligned}$$

and to its absorption operators:

$$\begin{aligned} \mathcal{J}_R^{(+)} &\equiv \lim_{\Delta t \rightarrow 0} \frac{\langle 0_{R,n}, 0_{L,n} | U_n | 1_{R,n}, 0_{L,n} \rangle}{\sqrt{\Delta t}} = -\sqrt{\gamma} s^\dagger s \otimes \sigma^\dagger, \quad (8) \\ \mathcal{J}_L^{(+)} &\equiv \lim_{\Delta t \rightarrow 0} \frac{\langle 0_{R,n}, 0_{L,n} | U_n | 0_{R,n}, 1_{L,n} \rangle}{\sqrt{\Delta t}} = -\sqrt{\gamma} s s^\dagger \otimes \sigma^\dagger. \end{aligned}$$

In the following we use the above operators to derive analytical expressions of the SPI wavefunctions with different initial conditions.

III. GENERATION OF PHOTON-NUMBER SUPERPOSITIONS

In this section, we benchmark the mapping of a qubit encoded in the QD's energy onto a flying qubit encoded in the

photon number:

$$(\alpha|e\rangle + \beta|g\rangle)|0\rangle \rightarrow |g\rangle(\alpha|1\rangle + \beta|0\rangle). \quad (9)$$

The energy qubit can be prepared using a classical pulse, and with the ideal map above, one can prepare any such superposition of 0- and 1-photon number states. Such a map does not require any external magnetic field, and in the ideal case, where the Overhauser field is also negligible, the action of the sole light-matter coupling for a time $t_\infty \gg \gamma^{-1}$ would give exactly Eq. (9) with $|1\rangle$ being either $|1_R\rangle = \sqrt{\gamma} \int_0^\infty dt' e^{-\gamma t'/2} b_R^\dagger(t')|0\rangle$, or $|1_L\rangle = \sqrt{\gamma} \int_0^\infty dt' e^{-\gamma t'/2} b_L^\dagger(t')|0\rangle$, according to the SPI's initial state being $|\uparrow\rangle \otimes (\alpha|e\rangle + \beta|g\rangle)$ or $|\downarrow\rangle \otimes (\alpha|e\rangle + \beta|g\rangle)$. In the following, without loss of generality for the analysis, we'll take the initial state $|\Psi_0^{(\uparrow)}\rangle = |\uparrow\rangle \otimes (\alpha|e\rangle + \beta|g\rangle)$, and hence $|1\rangle = |1_R\rangle$. We set $\Omega_e = 0$ and $\Omega_g = \Omega_O$ in the magnetic Hamiltonian H_s and compute the evolution of the SPI under the repeated action of the collision unitary [Eq. (4)] finding its state at time $t_\infty \gg \gamma^{-1}$ ($e^{-\gamma t_\infty/2} \approx 0$):

$$|\Psi_\infty^{(\uparrow)}\rangle = \left[\alpha \sum_{\mu=\uparrow,\downarrow} \int_0^\infty dt' f_{1_R}^{(\uparrow,\mu)}(t_\infty, t') b_R^\dagger(t') |\mu\rangle + \beta e^{-i\frac{\Omega_O t_\infty}{2} \mathbf{n} \cdot \mathbf{s}} |\uparrow\rangle \right] |0, g\rangle, \quad (10)$$

with

$$\begin{aligned} f_{1_R}^{(\uparrow,\uparrow)}(t, t') &= \langle g, \uparrow | \mathcal{K}(t-t') \mathcal{J}_R^{(-)} \mathcal{K}(t') | \uparrow, e \rangle \\ &= \sqrt{\gamma} e^{-\gamma t'/2} \left(\cos\left(\frac{\Omega_O(t-t')}{2}\right) - i \cos(\theta) \sin\left(\frac{\Omega_O(t-t')}{2}\right) \right) \end{aligned} \quad (11)$$

and

$$\begin{aligned} f_{1_R}^{(\uparrow,\downarrow)}(t, t') &= \langle g, \downarrow | \mathcal{K}(t-t') \mathcal{J}_R^{(-)} \mathcal{K}(t') | \uparrow, e \rangle \\ &= -i \sqrt{\gamma} e^{i\phi} \sin(\theta) e^{-\gamma t'/2} \sin\left(\frac{\Omega_O(t-t')}{2}\right), \end{aligned} \quad (12)$$

where the operators \mathcal{K} and $\mathcal{J}_R^{(-)}$ are given in Eq. (6) and Eq. (7) and the explicit expressions of all coefficients $f_j^{(\zeta,\mu)}(t, t')$ are given in Appendix A. Notice that, due to the Overhauser field, $|\Psi_\infty^{(\uparrow)}\rangle$ is an entangled spin-photon state. Its generation can be interpreted as follows: a spontaneous emission event (jump) turns on the precession of the electron spin due to the Overhauser field, since the jump can occur at any time between 0 and t_∞ , the wavefunction is a coherent superposition of jumps occurring at different times followed by electron spin precessions starting at that time. Then, to compare the performance against the ideal map [Eq. (9)], we first trace the realistic state over the spin degree of freedom obtaining the partially mixed state $\text{Tr}_{\text{spin}} [|\Psi_\infty^{(\uparrow)}\rangle \langle \Psi_\infty^{(\uparrow)}|] \equiv \rho_\infty$. We then compute its fidelity with the ideal state appearing in the right member of Eq. (9):

$$\begin{aligned} \mathcal{F}_{\text{PNS}}(\alpha, \beta) &= \langle \Psi_{\text{ideal}} | \rho_\infty | \Psi_{\text{ideal}} \rangle \\ &= \frac{|\alpha|^4 + 2|\alpha|^2|\beta|^2}{1 + \left(\frac{\Omega_O}{2\gamma}\right)^2} + |\beta|^4, \end{aligned} \quad (13)$$

where PNS stands for photon number superposition. The above expression is explicitly derived in Appendix B. Note that, if we started from the state $|\downarrow\rangle \otimes (\alpha|e\rangle + \beta|g\rangle)$, hence obtaining a left-circularly polarized photon instead of a right-circularly polarized one, the fidelity would have been the same, as shown in Appendix B. To get rid of the fidelity's dependence on the choice of the parameters α and β , we can integrate $\mathcal{F}_{\text{PNS}}(\alpha, \beta)$ over the uniform measure of the energy qubit's Bloch sphere [32], obtaining:

$$\mathcal{F}_{\text{PNS}} = \frac{1 + \left(\frac{\Omega_O}{2\sqrt{3}\gamma}\right)^2}{1 + \left(\frac{\Omega_O}{2\gamma}\right)^2}. \quad (14)$$

Taking the statistical average of the above fidelity with the isotropic Gaussian distribution of standard deviation w , we obtain:

$$\begin{aligned} \overline{\mathcal{F}}_{\text{PNS}} &= \sqrt{\frac{2}{\pi w^6}} \int_0^\infty d\Omega_O e^{-\Omega_O^2/2w^2} \mathcal{F}_{\text{PNS}} \\ &= \frac{8(w/\gamma) + (w/\gamma)^3 - 8\sqrt{2\pi} e^{\frac{2}{(w/\gamma)^2}} \text{Erfc}\left[\frac{\sqrt{2}}{(w/\gamma)}\right]}{3(w/\gamma)^3}. \end{aligned} \quad (15)$$

The above expression is plotted in Fig. (2). As expected, it goes to one in the limit of infinite electrons spin relaxation-time $w/\gamma \rightarrow 0$, and it goes to $1/3$ in the opposite limit, where the electron spin relaxation is so fast that the average polarization reaches the value of $1/3$, before the spontaneous emission even begins. In state-of-the-art QD devices at cryogenic temperature (see for instance Refs. [15, 33]), γ^{-1} can reach the order of a few hundred picoseconds, while w^{-1} is typically of the order of nanoseconds, hence the ratio w/γ can vary between 0.01 and 0.1. As clear from Fig. (2), these values of w/γ give a fidelity above 99%, hence electron spin relaxation does not affect relevantly the generation of 0- and 1-photon states superpositions.

IV. PHOTON-PHOTON GATE

The simplest design of controlled-Z (CZ) photon-photon gate, as proposed in Ref. [3], exploits the phase shift acquired by a resonant photon in the scattering with a two-level atom. In the ideal case, of monochromatic photons, the phase acquired in the scattering is exactly π . This mechanism, in the SPI, gives rise to a spin-phase gate, \mathcal{H} , controlled by the presence of one circularly polarized photon:

$$\begin{aligned} |\uparrow\rangle|g\rangle|1_R\rangle &\xrightarrow{\mathcal{H}} -|\uparrow\rangle|g\rangle|1_R\rangle, \\ |\downarrow\rangle|g\rangle|1_R\rangle &\xrightarrow{\mathcal{H}} |\downarrow\rangle|g\rangle|1_R\rangle, \end{aligned} \quad (16)$$

and analogously for a left polarized photon exchanging the roles of $|\uparrow\rangle$ and $|\downarrow\rangle$. Then, as in the previous section, without loss of generality, from now on we will take the logical basis of the photons to be $|1_R\rangle = |1\rangle$ and $|0\rangle = |0\rangle$.

Let us briefly recall the ideal protocol which is schematically represented in figure Fig. (3). The electron spin is prepared in $|\downarrow_y\rangle = \frac{|\uparrow\rangle - i|\downarrow\rangle}{\sqrt{2}}$; then the first R-photon, namely the

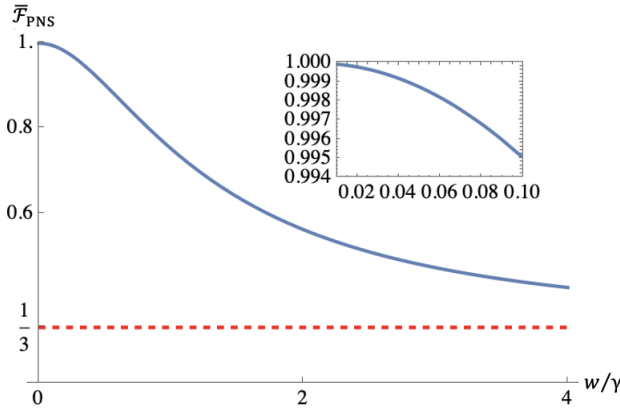


Figure 2: Fidelity of the superposition of 0- and 1-photon states varying the spin relaxation time w^{-1} with respect to the trion's lifetime. The plotted function is given in Eq. (15). State of the art QD devices having w/γ between 0.01 and 0.1 correspond to a nearly unitary fidelity (see the inset).

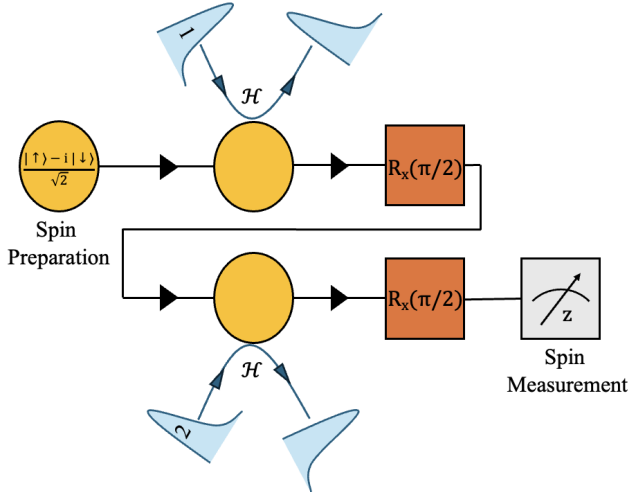


Figure 3: Schematic representation of a CZ photonic gate. The states of both control and target photons are arbitrary superpositions of 0– and 1–photon states. The electron spin is prepared in $|\downarrow_y\rangle$ and it interacts with the two photons via the spin-selective phase mapping, \mathcal{H} , given in Eq. (16). After interacting with each photon, a $\pi/2$ rotation around the x axis is performed on the electron spin. The spin-photon-photon state is given at this stage by Eq. (18). The electron spin is then measured, projecting the evolution onto a CZ gate up to a single photon unitary (see text).

control qubit, is sent in the SPI which scatters it according to Eq. (16); then a $\pi/2$ rotation around the x axis, $R_x(\pi/2)$, is applied on the electron spin:

$$|\downarrow_y\rangle(\alpha_1|0\rangle_1 + \beta_1|1\rangle_1) \xrightarrow{R_x(\pi/2)\mathcal{H}_1} -(i\alpha_1|0\rangle_1|\downarrow\rangle + \beta_1|1\rangle_1|\uparrow\rangle), \quad (17)$$

then the second R-photon, namely the target, is sent in the SPI followed by a second $R_x(\pi/2)$ rotation:

$$\begin{aligned}
& \left| \downarrow_y \right\rangle (\alpha_1 |0\rangle_1 + \beta_1 |1\rangle_1) (\alpha_2 |0\rangle_2 + \beta_2 |1\rangle_2) \xrightarrow{R_x(\pi/2) \mathcal{H}_2 R_x(\pi/2) \mathcal{H}_1} \\
& - \frac{1}{\sqrt{2}} |\uparrow\rangle [\alpha_1 \alpha_2 |0\rangle_1 |0\rangle_2 + \alpha_2 \beta_1 |1\rangle_1 |0\rangle_2 \\
& + \alpha_1 \beta_2 |0\rangle_1 |1\rangle_2 - \beta_1 \beta_2 |1\rangle_1 |1\rangle_2] \\
& - \frac{i}{\sqrt{2}} |\downarrow\rangle [\alpha_1 \alpha_2 |0\rangle_1 |0\rangle_2 - \alpha_2 \beta_1 |1\rangle_1 |0\rangle_2 \\
& + \alpha_1 \beta_2 |0\rangle_1 |1\rangle_2 + \beta_1 \beta_2 |1\rangle_1 |1\rangle_2]. \tag{18}
\end{aligned}$$

Let us notice that, in this ideal protocol, each photon scattering corresponds to the application of a spin-phase gate \mathcal{H} [Eq. (16)], subscripts 1 and 2 referring to first and second photon. At the end of this sequence, the electron spin is measured in the z direction. If it is found in $|\uparrow\rangle$, the photons have undergone the CZ gate, if it is found in $|\downarrow\rangle$, a Z gate must be applied to the control photon. In the following, for simplicity, we will compute the fidelity of the gate in the case where the final spin measurement projects it on $|\uparrow\rangle$.

In a realistic implementation, the spin cannot be manipulated unitarily between the single-photon scatterings, as no external magnetic field could be turned on and off instantaneously. Thus, the realistic protocol entails: turning on a transverse magnetic field, preparing the spin in the state $|\downarrow_y\rangle$, sending the control photon to the emitter (while the magnetic field is still on), letting the system evolve for a time $T_g = \pi/(2\Omega_g)$, then sending the target photon, let the SPI evolve for another time interval T_g . Notice that in the following we assume that the scattering of the first photon is completed before the second photon arrives in the SPI. We then look for the final SPI state in the long-time limit (when the scattering is completed), starting from the initial states $|\chi_0^{(\zeta)}\rangle = |\zeta, g, 1_R\rangle$, with $\zeta = \uparrow, \downarrow$ and $|1_R\rangle = \int_0^\infty dt' \xi_R(t') b_R^\dagger(t') |0\rangle$ and $\int_0^\infty dt' |\xi_R(t')|^2 = 1$. Using the Kraus operators [Eqs. (6)-(8)] we obtain:

$$\left| \chi_{\infty}^{(\zeta)} \right\rangle = \sum_{\mu=\uparrow,\downarrow} \sum_{j=R,L} \int_0^{t_{\infty}} dt' \lambda_j^{(\zeta,\mu)}(t,t') b_j^{\dagger}(t') |0\rangle |\mu\rangle |g\rangle \quad (19)$$

with

$$\begin{aligned} \lambda_R^{(\zeta, \mu)}(t, t') &= \xi(t') \langle g, \mu | \mathcal{K}(t) | \zeta, g \rangle \\ &+ \int_0^{t'} dt'' \xi(t'') \langle g, \mu | \mathcal{K}(t-t') \mathcal{J}_R^{(-)} \mathcal{K}(t'-t'') \mathcal{J}_R^{(+)} \mathcal{K}(t'') | \zeta, g \rangle \end{aligned} \quad (20)$$

and

$$\begin{aligned} & \lambda_L^{(\zeta, \mu)}(t, t') \\ &= \int_0^{t'} dt'' \xi(t'') \langle g, \mu | \mathcal{K}(t - t') \mathcal{J}_L^{(-)} \mathcal{K}(t' - t'') \mathcal{J}_R^{(+)} \mathcal{K}(t'') | \zeta, g \rangle, \end{aligned} \quad (21)$$

the explicit expressions of the coefficients $\lambda_R^{(\zeta, \mu)}(t, t')$ are given in Appendix A. The assumption that the scattering of the first

photon is completed before arrival of the second, implies that photons 1 and 2 have support on different time-bins modes, resp. $[0, T_g]$ and $[T_g, 2T_g]$, and we just need to combine two copies of Eq. (19) to get the SPI state at the end of the realistic protocol, $t = 2T_g$:

$$\begin{aligned} |\Phi(2T_g)\rangle &= -\frac{\alpha_1\alpha_2}{\sqrt{2}} |0\rangle_1 |0\rangle_2 (C_- |\uparrow\rangle + iC_+ |\downarrow\rangle) \\ &+ \frac{\alpha_2\beta_1}{\sqrt{2}} |0\rangle_2 \sum_{j,\mu} (\left| \omega_j^{(\uparrow,\mu)} \right\rangle_1 - i \left| \omega_j^{(\downarrow,\mu)} \right\rangle_1) e^{\frac{-i\pi\mathbf{n}\cdot\mathbf{s}}{4}} |\mu\rangle \\ &+ \frac{\alpha_1\beta_2}{2} |0\rangle_1 \sum_{k,\nu} [(1 - C_-) \left| \omega_k^{(\uparrow,\nu)} \right\rangle_2 |\nu\rangle - i(1 + C_+) \left| \omega_k^{(\downarrow,\nu)} \right\rangle_2 |\nu\rangle] \\ &+ \frac{\beta_1\beta_2}{\sqrt{2}} \sum_{k,j,\mu,\nu} (\left| \omega_k^{(\mu,\nu)} \right\rangle_2 \left| \omega_j^{(\uparrow,\mu)} \right\rangle_1 - i \left| \omega_k^{(\mu,\nu)} \right\rangle_2 \left| \omega_j^{(\downarrow,\mu)} \right\rangle_1) |\nu\rangle, \end{aligned} \quad (22)$$

where $C_- = \sin(\theta)e^{-i\phi} + i \cos(\theta)$, $C_+ = \sin(\theta)e^{i\phi} + i \cos(\theta)$,

$$\left| \omega_j^{(\mu,\nu)} \right\rangle_1 := \int_0^{T_g} ds \lambda_j^{(\mu,\nu)}(T_g, s) b_j^\dagger(s) |0\rangle, \quad (23)$$

and

$$\left| \omega_j^{(\mu,\nu)} \right\rangle_2 := \int_{T_g}^{2T_g} ds \lambda_j^{(\mu,\nu)}(T_g, s - T_g) b_j^\dagger(s) |0\rangle, \quad (24)$$

with μ, ν spanning the spin basis and j, k the photon polarization basis. In the rest of this section, we will consider the wavepackets of both input photons being decreasing exponentials, $\xi(t) := \sqrt{\Gamma} e^{-\frac{\Gamma t}{2}}$ with $T_g \gg \Gamma^{-1}$.

To compare the ideal protocol with the realistic one, we compute the fidelity of $|\Phi(2T_g)\rangle$ with the final state of the ideal gate [Eq. (18)]:

$$\mathcal{F}_{\text{CZ}}(\alpha, \beta) = \left| A|\alpha_1\alpha_2|^2 + B|\alpha_2\beta_1|^2 + C|\alpha_1\beta_2|^2 + D|\beta_1\beta_2|^2 \right|^2 \quad (25)$$

with

$$\begin{aligned} A &= C_-; \\ B &= \frac{(-\Lambda^{(\uparrow,\uparrow)} + i\Lambda^{(\downarrow,\uparrow)})(1 - i \cos(\theta))}{\sqrt{2}} \\ &+ \frac{(\Lambda^{(\downarrow,\downarrow)} + i\Lambda^{(\uparrow,\downarrow)}) \sin(\theta) e^{-i\phi}}{\sqrt{2}}; \\ C &= \frac{(C_- - 1)\Lambda^{(\uparrow,\uparrow)} + i(1 + C_+)\Lambda^{(\downarrow,\uparrow)}}{\sqrt{2}}; \\ D &= \Lambda^{(\uparrow,\downarrow)}\Lambda^{(\downarrow,\uparrow)} + \Lambda^{(\uparrow,\uparrow)}\Lambda^{(\uparrow,\downarrow)} - i\Lambda^{(\downarrow,\downarrow)}\Lambda^{(\downarrow,\uparrow)} - i\Lambda^{(\downarrow,\uparrow)}\Lambda^{(\uparrow,\downarrow)}; \end{aligned} \quad (26)$$

and

$$\Lambda^{(\mu,\nu)} := \int_0^{T_g} ds \xi^*(s) \lambda_R^{(\mu,\nu)}(T_g, s) \quad (27)$$

being the overlap between the input and the output photons wavepackets.

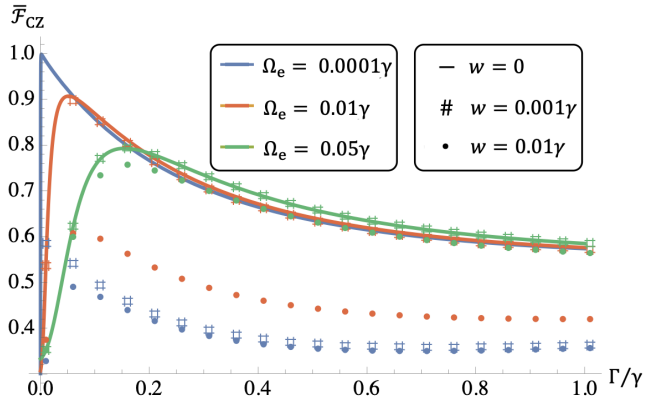


Figure 4: Fidelity of the CZ photon-photon gate varying the photons' bandwidth Γ for different values of the external magnetic field $\hbar\Omega_e/(g_{\text{tr}}\mu_B) = B^{\text{ext}}$, and of the spin relaxation time w^{-1} . The curves are obtained from the numerical integration of Eq. (28) with Overhauser field distribution of width w setting $\Omega_e = \bar{\Omega}_g$ (see the text).

As before, we eliminate the fidelity's dependence on the choice of the photons initial states, namely the parameters $\alpha \equiv (\alpha_1; \alpha_2)$ and $\beta \equiv (\beta_1, \beta_2)$, by integrating $\mathcal{F}_{\text{CZ}}(\alpha, \beta)$ over the uniform measures of their Bloch spheres:

$$\begin{aligned} \mathcal{F}_{\text{CZ}} &= \frac{1}{9}(|A|^2 + |B|^2 + |C|^2 + |D|^2) + \\ &\quad \frac{1}{18}(AB^* + AC^* + BD^* + CD^* + h.c.) + \\ &\quad \frac{1}{36}(AD^* + BC^* + h.c.). \end{aligned} \quad (28)$$

The above expression shows that, as soon as $A = B = C = D = e^{i\phi}$, the fidelity goes to one. As shown in Appendix C, this condition is always verified in the ideal protocol: no Overhauser field, i.e. $\mathbf{n} = \hat{x}$ and $\Omega_e = \Omega_g$; monochromatic photons, i.e. $\Gamma/\gamma \approx 0$; instantaneous spontaneous emission, i.e. $\gamma/\Omega_g \approx 0$; then summarizing, the realistic protocol converges to the ideal one when $\gamma \gg \Gamma \gg \Omega_g \approx \Omega_e$.

Aside from the ideal limit, we account for the Overhauser field's randomness, as before, via statistical average with the Gaussian distribution of width w . Due to the external magnetic field, this time the center of the Gaussian distribution of the electron spin precession frequencies is different from zero, we denote it with $\bar{\Omega}_g$. The fidelity is plotted in Fig. (4) as a function of the bandwidth Γ/γ for different values of $\Omega_e = \bar{\Omega}_g$. The plot shows that, as expected from the chain of inequalities $\gamma \gg \Gamma \gg \Omega_e$, by increasing the magnitude of the external magnetic field $\hbar\Omega_e/(g_{\text{tr}}\mu_B) = B^{\text{ext}}$, the maximum of the fidelity moves towards greater values of the photons' bandwidth Γ/γ . Notice that such dependence on the incoming photons bandwidth can only be captured by a model that goes beyond the monochromatic approximation.

The plot also shows that when the Overhauser field is taken into account, an optimal performance requires $\Omega_e = \bar{\Omega}_g \gg w$, this reflects the fact that the detrimental impact of the Overhauser field becomes negligible in a strong external field. In

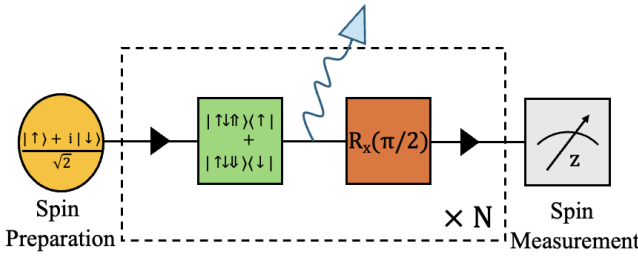


Figure 5: Schematic representation of the Lindner-Rudolph protocol. The electron spin is prepared in $|\uparrow_y\rangle$. Then a "unit step" is performed N times to generate an entangled state of N photons plus spin. The unit step consists of a classical excitation of the QD, followed by spontaneous emission, followed by a $\pi/2$ rotation of the electron spin around the x axis. The joint state of the spin and the N photons is given by Eq. (31). After this the spin is measured and disentangled from the N photons resulting in an N photon cluster state.

a realistic SPI, where the spin decoherence rate w is fixed by the QD structure, this optimization can only be achieved by increasing the external magnetic field. At the same time, however, Ω_e must remain smaller than the photon bandwidth Γ that in turn must be smaller than the spontaneous emission rate γ , making this optimization very challenging. As shown in the plot, in order to obtain a fidelity close to 90%, in the absence of Overhauser field, one needs to work with a spin precession frequency at least two orders of magnitude smaller than the spontaneous emission rate (blue and orange lines in figure). However, with such a weak external field, the presence of even a very small Overhauser field is highly detrimental for the gate performance. Our results show that, even in the best-case scenario of a SPI having a decoherence rate 100 times smaller than the spontaneous emission rate, the fidelity barely reaches 0.8 (green line).

V. LINDNER-RUDOLPH PROTOCOL FOR CLUSTER STATES GENERATION

A. The ideal protocol

The Lindner-Rudolph (LR) protocol generates linear clusters of propagating photons entangled in polarization, having, in principle, arbitrary length [5]. Each photon of the cluster is generated by an instantaneous excitation of the QD's energy levels followed by spontaneous emission and spin precession. A cluster of N photons is then generated by N repetitions of this unit step as shown in Fig. (5). In the ideal protocol, the sequence starts with the SPI prepared in the trion spin superposition state, $|\Psi(0)\rangle = |\uparrow_y\rangle|e\rangle$, where $|\uparrow_y\rangle = (|\uparrow\rangle + i|\downarrow\rangle)/\sqrt{2}$. Then the spontaneous emission, considered as instantaneous with respect to the electron spin precession, creates a maximally entangled spin-photon state, $|\Psi(0^+)\rangle = |g\rangle(|\uparrow, 1_R\rangle + i|\downarrow, 1_L\rangle)/\sqrt{2}$. In the ideal protocol, there is no Overhauser field and electron and trion have equal

Landé factors, i.e. $\Omega_g = \Omega_e = \Omega$ and $\mathbf{n} = \{1, 0, 0\}$, hence the action of H_s for a time $T_1 = \pi/(2\Omega)$ implements a rotation on the spin qubit of an angle $\pi/2$ around the x axis. The SPI wavefunction at time $t = T_1$ is then

$$|\Psi_1\rangle = \frac{1}{\sqrt{2}}|g\rangle(|\uparrow_y\rangle|1_L\rangle_1 + |\downarrow_y\rangle|1_R\rangle_1), \quad (29)$$

where $|1_R(L)\rangle_1 = \sqrt{\gamma} \int_0^{T_1} dt e^{-\gamma t/2} b_{R(L)}^\dagger(t)|0\rangle$ is a single-photon state normalized in $[0, T_1]$, condition guaranteed by the assumption of instantaneous emission i.e. $\Omega/\gamma \approx 0$ ($e^{-\gamma T_1} \approx 0$). Then a classical pulse re-excites the QD such that a second photon is emitted followed by another spin precession for time interval equal to T_1 . The state at $t = 2T_1$ is then

$$|\Psi_2\rangle = \frac{1}{2}|g\rangle(|\downarrow_y\rangle|1_R\rangle_1|1_R\rangle_2 + |\downarrow_y\rangle|1_L\rangle_1|1_R\rangle_2 - |\uparrow_y\rangle|1_R\rangle_1|L_R\rangle_2 + |\uparrow_y\rangle|1_L\rangle_1|1_L\rangle_2), \quad (30)$$

where the subscript 2 means that the photon's state has support in $[T_1, 2T_1]$. The wavefunction of the joint system after N repetitions of the ideal unit step can be written in the compact matrix product form:

$$|\Psi_N\rangle = |g\rangle \left(\begin{smallmatrix} \frac{1}{\sqrt{2}} & \frac{i}{\sqrt{2}} \end{smallmatrix} \right) \cdot (\mathcal{W}_1 \cdot \mathcal{W}_2 \cdot \dots \cdot \mathcal{W}_N) \cdot \left(\begin{smallmatrix} |\uparrow\rangle \\ |\downarrow\rangle \end{smallmatrix} \right) \quad (31)$$

$$\equiv |g\rangle \left(\begin{smallmatrix} \frac{1}{\sqrt{2}} & \frac{i}{\sqrt{2}} \end{smallmatrix} \right) \prod_{j=1}^N (\mathcal{W}_j) \left(\begin{smallmatrix} |\uparrow\rangle \\ |\downarrow\rangle \end{smallmatrix} \right)$$

with

$$\mathcal{W}_m = \frac{1}{\sqrt{2}} \begin{pmatrix} |1_R\rangle_m & -i|1_R\rangle_m \\ -i|1_L\rangle_m & |1_L\rangle_m \end{pmatrix} \quad (32)$$

The row vector in the matrix product is the initial state of the spin, in this case $|\uparrow_y\rangle$, with $|\uparrow\rangle = (1 \ 0)$, $|\downarrow\rangle = (0 \ 1)$.

In the Lindner-Rudolph seminal paper, the authors consider the deviation from the ideal protocol due to a finite ratio Ω/γ . This deviation can be linked to a fundamental no-go theorem of quantum mechanics, known as WAY theorem [34]. WAY theorem says that it is impossible to obtain a perfect one-to-one mapping between two interacting quantum systems when their interaction Hamiltonian does not commute with their full Hamiltonian. As H_s does not commute with $V_I(t)$, the mapping $|\uparrow(\downarrow)\rangle \rightarrow |1_{R(L)}\rangle$ cannot be perfect. Lindner and Rudolph showed that, for $\Omega_e = \Omega_g = \Omega$ and $w/\gamma \approx 0$, the sole effect of the finite ratio $\Omega/\gamma \neq 0$ induces a X Pauli error on the spin qubit. In the next section we show that our Hamiltonian approach gives the same result. As for the spin decoherence induced by the Overhauser field, they model it as a further X Pauli error on the spin qubit whose probability depends solely on w/γ . In their top-down approach, the overall error probability of the protocol's unit step is the product of the probabilities of the two errors considered as independent. As we show in the next section, our microscopic model allows us to go beyond this approximation, and it also accounts naturally for the loss of fidelity due to deformations of the photonic wavepackets.

B. Realistic Hamiltonian model

Throughout this section, we will assume that the classical pulse exciting the QD is linearly polarized and very short with respect to the trion's lifetime, hence producing a nearly instantaneous population swap from electron to trion for both spin projections. Let us notice that, as mentioned in Sec. II, recent experimental results [25] show that a suitable tuning of the angle between the pulse's linear polarization and the magnetic field direction is needed to obtain a constant and positive value of Ω_e as assumed in this paper. Furthermore, we consider the time $T_1 = \pi/(2\Omega_g)$ of each electron spin precession to be longer than the trion's lifetime, yet keeping their ratio finite. We can then write the SPI wavefunction after N repetitions of the realistic unit step as:

$$|\Psi(NT_1)\rangle = |g\rangle \left(\frac{1}{\sqrt{2}} \quad \frac{i}{\sqrt{2}} \right) \prod_{m=1}^N (W_m) \begin{pmatrix} |\uparrow\rangle \\ |\downarrow\rangle \end{pmatrix} \quad (33)$$

with

$$W_m = \begin{pmatrix} \sum_{i=R,L} \langle \Phi_i^{(\uparrow,\uparrow)} \rangle_m & \sum_{i=R,L} \langle \Phi_i^{(\uparrow,\downarrow)} \rangle_m \\ \sum_{i=R,L} \langle \Phi_i^{(\downarrow,\uparrow)} \rangle_m & \sum_{i=R,L} \langle \Phi_i^{(\downarrow,\downarrow)} \rangle_m \end{pmatrix} \quad (34)$$

where we defined the un-normalized field's wavefunctions as:

$$\langle \Phi_i^{(\zeta,\mu)} \rangle_m = \int_{(m-1)T_1}^{mT_1} dt f_i^{(\zeta,\mu)}(mT_1, t + T_1 - mT_1) b_i^\dagger(t) |0\rangle; \quad (35)$$

the subscript m refers to the fact that the photon is emitted in the interval $[(m-1)T_1, mT_1]$, and the coefficients $f_i^{(\zeta,\mu)}(t, t')$ are given in Appendix A. Notice that, in the ideal protocol, the field's states $|\Phi_L^{(\uparrow,\mu)}\rangle$ and $|\Phi_R^{(\downarrow,\zeta)}\rangle$ are never populated for any $\mu, \zeta = \uparrow, \downarrow$. The probability to find a photon in these states corresponds to the conditional probabilities of detecting an L (R) photon after preparing the spin in $|\uparrow\rangle$ ($|\downarrow\rangle$), namely $P(\downarrow|R) = P(\uparrow|L)$ where $P(\zeta|j) = \sum_\mu \langle \Phi_j^{(\zeta,\mu)} | \Phi_j^{(\zeta,\mu)} \rangle$, it reads

$$P(\downarrow|R) = P(\uparrow|L) = \frac{(\Omega_e/\gamma)^2}{2[1 + (\Omega_e/\gamma)^2]}. \quad (36)$$

The above expression is the probability derived by Lindner and Rudolph in their seminal paper for the bit-flip (X Pauli) error as mentioned in the previous subsection.

Using the matrix product form of the ideal and the real state, it is possible to find a compact expression for the real state fidelity after N iterations of the protocol. Assuming that the final spin measurement is perfectly projective, the fidelity is given by the modulus square of the states overlap, that can be written as:

$$\langle \Psi(NT_1) | \Psi_N \rangle = \left(\frac{1}{\sqrt{2}} \quad \frac{i}{\sqrt{2}} \right) \left(\prod_{m=1}^N \mathcal{W}_m \right) \left(\prod_{m=1}^N W_m \right)^\dagger \begin{pmatrix} \frac{1}{\sqrt{2}} \\ \frac{-i}{\sqrt{2}} \end{pmatrix} \quad (37)$$

where again the first and the last vectors correspond to the state of the spin at $t = 0$.

The above expression shows that for any number of iterations the fidelity can be derived by combining suitably the 8 overlaps :

$$O_j^{(\zeta,\mu)} = \langle \mathbf{1}_j | \Phi_j^{(\zeta,\mu)} \rangle = \int_0^{T_1} dt \sqrt{\gamma} e^{-\gamma t/2} f_j^{(\zeta,\mu)*}(T_1, t). \quad (38)$$

For instance, using Eq. (37) is easy to find that the fidelity at time T_1 :

$$\begin{aligned} \mathcal{F}_{LR}^{(1)} &= |\langle \Psi_1 | \Psi(T_1) \rangle|^2 \\ &= \frac{1}{2\sqrt{2}} |O_R^{(\uparrow,\uparrow)} + O_L^{(\uparrow,\uparrow)} + iO_R^{(\uparrow,\downarrow)} - iO_L^{(\uparrow,\downarrow)} \\ &\quad + iO_R^{(\downarrow,\uparrow)} + iO_L^{(\downarrow,\uparrow)} - O_R^{(\downarrow,\downarrow)} + O_L^{(\downarrow,\downarrow)}|^2 \end{aligned} \quad (39)$$

Similarly the fidelity after 2 iterations is:

$$\begin{aligned} \mathcal{F}_{LR}^{(2)} &= |\langle \Psi_2 | \Psi(2T_1) \rangle|^2 \\ &= \left| \frac{1}{4} \sum_{\mu=\uparrow,\downarrow} [(O_R^{(\uparrow,\mu)} + iO_R^{(\downarrow,\mu)}) (O_R^{(\mu,\uparrow)} - O_L^{(\mu,\uparrow)} + iO_R^{(\mu,\downarrow)} + iO_L^{(\mu,\downarrow)}) \right. \\ &\quad \left. + (O_L^{(\uparrow,\mu)} + iO_L^{(\downarrow,\mu)}) (O_R^{(\mu,\uparrow)} + O_L^{(\mu,\uparrow)} + iO_R^{(\mu,\downarrow)} - iO_L^{(\mu,\downarrow)})] \right|^2 \end{aligned} \quad (40)$$

In the absence of Overhauser noise, setting $\mathbf{n} = \hat{x}$ and $\Omega_g = k\Omega_e$ with $k = g_{\text{el}}/g_{\text{tr}}$ being the ratio between electron and trion Landé factors, it is possible to find a compact expression for the fidelity after the j -th step (at time $t = jT_1$) that we denote $\mathcal{F}_{LR,id}^{(j)}$:

$$\mathcal{F}_{LR,id}^{(j)} = \mathcal{F}_{LR,id}^{(1)} f^{j-1} + O(\Omega_e^4/\gamma^4) \quad (41)$$

with

$$\mathcal{F}_{LR,id}^{(1)} = \left[1 - \left(\frac{1+k^2}{2} \right) P(\downarrow|R) \right]^2 + O(\Omega_e^4/\gamma^4), \quad (42)$$

and

$$f := \frac{\mathcal{F}_{LR,id}^{(2)}}{\mathcal{F}_{LR,id}^{(1)}} = \left[1 - \frac{(1-k+k^2)}{2} P(\downarrow|R) \right]^2 + O(\Omega_e^4/\gamma^4) \quad (43)$$

The above expression, for $k = 1$, gives the fidelity obtained in the seminal paper using the bit-flip error. Setting experimentally realistic values, such as $k = 2$ and $\Omega_e/\gamma = 0.1$, it gives a fidelity above 75% for up to 15 photons.

As in the previous sections, we finally account for the presence of the Overhauser field by taking the statistical average of the fidelities [Eq. (39) and Eq. (40)] with the isotropic Gaussian distribution of width w . The curves, obtained via numerical integration, are shown in Fig. (6). The plots show clearly that the Overhauser field affects the fidelity significantly only when w becomes comparable with Ω_e i.e. when the Overhauser field cannot be treated as a small perturbation of the external field. Thus the optimal value of

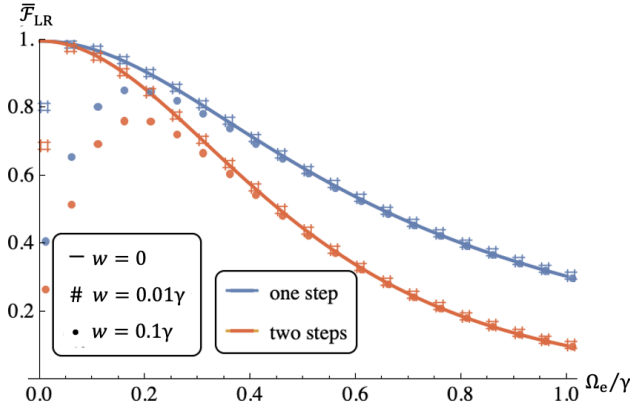


Figure 6: Fidelity of the final states of LR protocol after one (blue) and two (orange) unit steps. The curves are obtained respectively from the numerical integration of Eq. (39) and Eq. (40) with Overhauser field distribution of width w setting $\bar{\Omega}_g = 2\Omega_e$, and varying Ω_e .

the tunable parameter Ω_e depends on the spin decoherence rate w of the device.

Let us notice that, at the working point of Ref. [15], $k = 2$, $\Omega_e/\gamma \approx 0.2$ and $w/\gamma \approx 0.1$, our curves (dotted data sets) predict $\bar{\mathcal{F}}^{(1)}_{LR} = 0.85$ and $\bar{\mathcal{F}}^{(2)}_{LR} = 0.76$. These values, as expected, are slightly bigger than those reported in the experimental paper, resp. 0.8 and 0.63. We then conclude that our model is suitably tailored to predict fidelity upper bounds of the Lindner-Rudolph protocol in realistic QD SPIs. We see that for realistic values of w/γ we can tune the magnetic field to obtain fidelities between 0.9 – 0.99 for $N = 1, 2$. Using the slight underestimate of $p = 0.01$ error per unit step, such cluster states are sufficient for fault tolerant quantum computation [35].

VI. CONCLUSION

We solved the Hamiltonian dynamics of a QD SPI interacting with photonic wavepackets in the presence of magnetic fields. We model the solid-state SPI as a degenerate four level system in the absence of external fields where the ground states correspond to orthogonal projections of an electron spin and the excited states to those of a trion spin. Our approach considers both an external tunable magnetic field, and an Overhauser field, namely the effective magnetic field modeling the electron's hyperfine interaction with the nuclei of the atoms forming the QD. Following the seminal Merkulov-Efros-Rosen semiclassical model, the latter is treated as a static isotropic white noise, and we account for its randomness by taking statistical averages of the quantum

mechanical observables over all its possible configurations, with the spin relaxation rate then given by the width of the white noise distribution. Varying this parameter, all along the paper, we range from idealized (noiseless) to state-of-the-art conditions. Using this model, we analytically evaluated the performance of three key technological tasks achievable with the SPI: generation of coherent superpositions of 0- and 1-photon states, photon-photon controlled Z gate, and the Lindner-Rudolph protocol to generate linear photonic clusters. Our results show that, under realistic conditions for state-of-the-art devices such as in [15, 16, 18], the SPI can generate arbitrary superpositions of 0- and 1-photon states with very high fidelity despite the intrinsic spin relaxation due to the Overhauser field. In contrast, the photon-photon gate is found to be extremely sensitive to the spin relaxation: it functions reliably only when the Overhauser field is absent, and is very challenging to optimize even when its intensity is one order of magnitude lower than in state-of-the-art devices. This is due to the fact that, on the one hand, noiseless photon-scattering (without wavepackets deformations) requires very long photons, and on the other hand, mitigation of the spin decoherence requires very short scattering dynamics. Finally, we show that the Lindner-Rudolph protocol for cluster-state generation is comparatively robust against spin relaxation. In [35] a measurement-based quantum computation model [36] has been proposed that is fault tolerant with very high thresholds. The resource states used are one dimensional cluster states, and using the error analysis from the seminal paper [5] it is found in simulations that the LR protocol is sufficiently robust to generate the required quality of cluster states for fault tolerant quantum computation. The present analysis can be used to refine such simulations by using more accurate resource states generated by the realistic LR protocol. Our results provide theoretical performance bounds for passive implementations indicating how active error-mitigation strategies could further enhance cluster-state quality if required. We conclude by noting that, even though the analysis was tailored for QD SPI, it holds for all systems with similar structure of the energy levels and selection rules. From a more general point of view, our results prove that adopting a Hamiltonian analysis is not only feasible, but fruitful for accurate benchmarking of protocols for computation with photons.

Acknowledgments – A.A., HKN, and TA acknowledge the National Research Foundation, Singapore through the National Quantum Office, hosted in A*STAR, under its Centre for Quantum Technologies Funding Initiative (S24Q2d0009). A.A. acknowledges the Plan France 2030 through the projects NISQ2LSQ (Grant ANR-22-PETQ-0006) and OQuLus (Grant ANR-22-PETQ-0013). TA and HKN are also supported in part by the NRF-ANR joint QuRes project (NRF2021-NRF-ANR005).

[1] H. J. Kimble, *Nature* **453**, 1023–1030 (2008).

[2] F. Ciccarello, P. Lodahl, and D. Schneble, *Opt. Photon. News* **35**, 34 (2024).

[3] C. Bonato, F. Haupt, S. S. R. Oemrawsingh, J. Gudat, D. Ding, M. P. van Exter, and D. Bouwmeester, *Physical Review Letters* **104**, 160503 (2010).

[4] C. Y. Hu, W. J. Munro, and J. G. Rarity, *Physical Review B* **78**, 125318 (2008), publisher: American Physical Society.

[5] N. H. Lindner and T. Rudolph, *Physical Review Letters* **103**, 113602 (2009).

[6] S. E. Economou and P. Dev, *Nanotechnology* **27**, 504001 (2016).

[7] H. Pichler, S. Choi, P. Zoller, and M. D. Lukin, *Proceedings of the National Academy of Sciences* **114**, 11362 (2017).

[8] T. Wilk, S. C. Webster, A. Kuhn, and G. Rempe, *Science* **317**, 488 (2007).

[9] P. Thomas, L. Ruscio, O. Morin, and G. Rempe, *Nature* **608**, 677 (2022).

[10] C.-W. Yang, Y. Yu, J. Li, B. Jing, X.-H. Bao, and J.-W. Pan, *Nature Photonics* **16**, 658 (2022).

[11] A. Stute, B. Casabone, P. Schindler, T. Monz, P. O. Schmidt, B. Brandstätter, T. E. Northup, and R. Blatt, *Nature* **485**, 482 (2012).

[12] W. B. Gao, P. Fallahi, E. Togan, J. Miguel-Sánchez, and A. Imamoglu, *Nature* **491**, 426 (2012).

[13] A. Javadi, D. Ding, M. H. Appel, S. Mahmoodian, M. C. Löbl, I. Söllner, R. Schott, C. Papon, T. Pregnolato, S. Stobbe, L. Middolo, T. Schröder, A. D. Wieck, A. Ludwig, R. J. Warburton, and P. Lodahl, *Nature Nanotechnology* **13**, 398 (2018), number: 5 Publisher: Nature Publishing Group.

[14] I. Schwartz, D. Cogan, E. R. Schmidgall, Y. Don, L. Gantz, O. Kenneth, N. H. Lindner, and D. Gershoni, *Science* **354**, 434 (2016).

[15] N. Coste, D. Fioretto, N. Belabas, S. Wein, P. Hilaire, R. Frantzeskakis, M. Gundin, B. Goes, N. Somaschi, M. Morassi, *et al.*, *Nature Photonics* **1** (2023).

[16] H. Huet, P. Ramesh, S. Wein, N. Coste, P. Hilaire, N. Somaschi, M. Morassi, A. Lemaître, I. Sagnes, M. Doty, *et al.*, *Nature communications* **16**, 4337 (2025).

[17] D. Cogan, Z.-E. Su, O. Kenneth, and D. Gershoni, *Nature Photonics* **17**, 324 (2023).

[18] M. Gundín, P. Hilaire, C. Millet, E. Mehdi, C. Antón, A. Harouri, A. Lemaître, I. Sagnes, N. Somaschi, O. Krebs, *et al.*, *Physical Review Letters* **134**, 036902 (2025).

[19] N. Somaschi, V. Giesz, L. De Santis, J. Loredo, M. P. Almeida, G. Hornecker, S. L. Portalupi, T. Grange, C. Anton, J. Demory, *et al.*, *Nature Photonics* **10**, 340 (2016).

[20] S. Thomas and P. Senellart, *Nature Nanotechnology* **16**, 367 (2021).

[21] B. Urbaszek, X. Marie, T. Amand, O. Krebs, P. Voisin, P. Maletinsky, A. Högele, and A. Imamoglu, *Rev. Mod. Phys.* **85**, 79 (2013).

[22] C. W. Gardiner and M. J. Collett, *Phys. Rev. A* **31**, 3761 (1985).

[23] C. Gardiner and P. Zoller, *Quantum noise: a handbook of Markovian and non-Markovian quantum stochastic methods with applications to quantum optics* (Springer Science & Business Media, 2004).

[24] P. Ramesh, E. Annoni, N. Margaria, D. Fioretto, A. Pishchagin, M. Morassi, A. Lemaître, M. Doty, P. Senellart, L. Lanco, N. Belabas, S. Wein, and O. Krebs, *Phys. Rev. Appl.* **24**, 024047 (2025).

[25] P. Ramesh, E. Annoni, N. Margaria, D. Fioretto, A. Pishchagin, M. Morassi, A. Lemaître, M. Doty, P. Senellart, L. Lanco, N. Belabas, S. Wein, and O. Krebs, *Phys. Rev. Appl.* **24**, 024047 (2025).

[26] I. A. Merkulov, A. L. Efros, and M. Rosen, *Phys. Rev. B* **65**, 205309 (2002).

[27] A. Bechtold, D. Rauch, F. Li, T. Simmet, P.-L. Ardelt, A. Reigler, K. Müller, N. A. Sinitzyn, and J. J. Finley, *Nature Physics* **11**, 1005 (2015).

[28] F. Ciccarello, *Quantum Measurements and Quantum Metrology* **4** (2017), 10.1515/qmetro-2017-0007.

[29] M. Maffei, P. A. Camati, and A. Auffèves, *Entropy* **24** (2022), 10.3390/e24020151.

[30] M. Maffei, B. O. Goes, S. C. Wein, A. N. Jordan, L. Lanco, and A. Auffèves, *Quantum* **7**, 1099 (2023).

[31] M. Maffei, D. Pomarico, P. Facchi, G. Magnifico, S. Pascazio, and F. V. Pepe, *Phys. Rev. Res.* **6**, L032017 (2024).

[32] M. A. Nielsen, *Physics Letters A* **303**, 249–252 (2002).

[33] S. C. Wein, J. C. Loredo, M. Maffei, P. Hilaire, A. Harouri, N. Somaschi, A. Lemaître, I. Sagnes, L. Lanco, O. Krebs, *et al.*, *Nature Photonics* **16**, 374 (2022).

[34] L. Loveridge and P. Busch, *The European Physical Journal D* **62**, 297 (2011).

[35] S. Paesani and B. J. Brown, *Phys. Rev. Lett.* **131**, 120603 (2023).

[36] H. J. Briegel, D. E. Browne, W. Dür, R. Raussendorf, and M. Van den Nest, *Nature Physics* **5**, 19 (2009).

Appendix A: Explicit expression of the spin-photon wavefunction

First we give the expressions for spontaneous emission. Note that when there are two time arguments, the first argument is the observation time and the second argument is the time mode described by the wave function:

$$\begin{aligned}
f_0^{(\zeta, \mu)} &= e^{-\frac{\gamma t}{2}} \left(\cos\left(\frac{\Omega_e t}{2}\right) \delta_{\mu, \zeta} - i \sin\left(\frac{\Omega_e t}{2}\right) (1 - \delta_{\mu, \zeta}) \right) \\
f_{1_R}^{(\uparrow, \uparrow)}(t, t') &= \sqrt{\gamma} e^{-\frac{1}{2}(\gamma t')} \cos\left(\frac{\Omega_e t'}{2}\right) \left(\cos\left(\frac{1}{2}\Omega_g(t - t')\right) - i n_z \sin\left(\frac{1}{2}\Omega_g(t - t')\right) \right) = \left(f_{1_L}^{(\downarrow, \downarrow)}(t, t')\right)^* \\
f_{1_R}^{(\uparrow, \downarrow)}(t, t') &= -i \sqrt{\gamma} (n_x + i n_y) e^{-\frac{1}{2}(\gamma t')} \cos\left(\frac{t' \Omega_e}{2}\right) \sin\left(\frac{1}{2}\Omega_g(t - t')\right) = -\left(f_{1_L}^{(\downarrow, \uparrow)}(t, t')\right)^* \\
f_{1_L}^{(\uparrow, \uparrow)}(t, t') &= i \sqrt{\gamma} (n_y + i n_x) e^{-\frac{1}{2}(\gamma t')} \sin\left(\frac{t' \Omega_e}{2}\right) \sin\left(\frac{1}{2}\Omega_g(t - t')\right) = \left(f_{1_R}^{(\downarrow, \downarrow)}(t, t')\right)^* \\
f_{1_L}^{(\uparrow, \downarrow)}(t, t') &= -i \sqrt{\gamma} e^{-\frac{1}{2}(\gamma t')} \sin\left(\frac{t' \Omega_e}{2}\right) \left(\cos\left(\frac{1}{2}\Omega_g(t - t')\right) + i n_z \sin\left(\frac{1}{2}\Omega_g(t - t')\right) \right) = -\left(f_{1_R}^{(\downarrow, \uparrow)}(t, t')\right)^*
\end{aligned}$$

The overlaps $O_j^{(\zeta, \mu)}$ are simply time integrals of these multiplied by $\sqrt{\gamma} e^{-\gamma t'/2}$ from 0 to $t := T_1 = \pi/(2\Omega_g^{(0)})$. Now we list the expressions for single-photon scattering.

$$\begin{aligned}
\lambda_R^{(\uparrow, \uparrow)}(t, t') &= \xi(t') \left[\cos\left(\frac{\Omega_g t}{2}\right) - i n_z \sin\left(\frac{\Omega_g t}{2}\right) \right] \\
&\quad - \gamma \left[\cos\left(\frac{\Omega_g(t - t')}{2}\right) - i n_z \sin\left(\frac{\Omega_g(t - t')}{2}\right) \right] \int_0^{t'} dt'' \xi(t'') e^{-\frac{\gamma(t'' - t')}{2}} \cos\left(\frac{\Omega_e(t' - t'')}{2}\right) \left[\cos\left(\frac{\Omega_g t''}{2}\right) - i n_z \sin\left(\frac{\Omega_g t''}{2}\right) \right] \\
\lambda_R^{(\downarrow, \uparrow)}(t, t') &= -i \xi(t') \left[n_x - i n_y \right] \sin\left(\frac{\Omega_g t}{2}\right) \\
&\quad + i \gamma \left[\cos\left(\frac{\Omega_g(t - t')}{2}\right) - i n_z \sin\left(\frac{\Omega_g(t - t')}{2}\right) \right] \int_0^{t'} dt'' \xi(t'') e^{-\frac{\gamma(t'' - t')}{2}} \cos\left(\frac{\Omega_e(t' - t'')}{2}\right) \left[n_x - i n_y \right] \sin\left(\frac{\Omega_g t''}{2}\right) \\
\lambda_R^{(\uparrow, \downarrow)}(t, t') &= -i \xi(t') \left[n_x + i n_y \right] \sin\left(\frac{\Omega_g t}{2}\right) \\
&\quad + i \gamma \left[n_x + i n_y \right] \sin\left(\frac{\Omega_g(t - t')}{2}\right) \int_0^{t'} dt'' \xi(t'') e^{-\frac{\gamma(t'' - t')}{2}} \cos\left(\frac{\Omega_e(t' - t'')}{2}\right) \left[\cos\left(\frac{\Omega_g t''}{2}\right) - i n_z \sin\left(\frac{\Omega_g t''}{2}\right) \right] \\
\lambda_R^{(\downarrow, \downarrow)}(t, t') &= \xi(t') \left[\cos\left(\frac{\Omega_g t}{2}\right) - i n_z \sin\left(\frac{\Omega_g t}{2}\right) \right] \\
&\quad + i \gamma \left[n_x^2 + n_y^2 \right] \sin\left(\frac{\Omega_g(t - t')}{2}\right) \int_0^{t'} dt'' \xi(t'') e^{-\frac{\gamma(t'' - t')}{2}} \cos\left(\frac{\Omega_e(t' - t'')}{2}\right) \sin\left(\frac{\Omega_g t''}{2}\right) \\
\lambda_L^{(\uparrow, \uparrow)}(t, t') &= \gamma \left[n_x - i n_y \right] \sin\left(\frac{\Omega_g(t - t')}{2}\right) \int_0^{t'} dt'' \xi(t'') e^{-\frac{\gamma(t'' - t')}{2}} \sin\left(\frac{\Omega_e(t' - t'')}{2}\right) \left[\cos\left(\frac{\Omega_g t''}{2}\right) - i n_z \sin\left(\frac{\Omega_g t''}{2}\right) \right] \\
\lambda_L^{(\downarrow, \uparrow)}(t, t') &= -i \gamma \left[n_x - i n_y \right]^2 \sin\left(\frac{\Omega_g(t - t')}{2}\right) \int_0^{t'} dt'' \xi(t'') e^{-\frac{\gamma(t'' - t')}{2}} \sin\left(\frac{\Omega_e(t' - t'')}{2}\right) \sin\left(\frac{\Omega_g t''}{2}\right) \\
\lambda_L^{(\uparrow, \downarrow)}(t, t') &= i \gamma \left[\cos\left(\frac{\Omega_g(t - t')}{2}\right) + i n_z \sin\left(\frac{\Omega_g(t - t')}{2}\right) \right] \int_0^{t'} dt'' \xi(t'') e^{-\frac{\gamma(t'' - t')}{2}} \sin\left(\frac{\Omega_e(t' - t'')}{2}\right) \left[\cos\left(\frac{\Omega_g t''}{2}\right) - i n_z \sin\left(\frac{\Omega_g t''}{2}\right) \right] \\
\lambda_L^{(\downarrow, \downarrow)}(t, t') &= \gamma \left(n_x - i n_y \right) \left[\cos\left(\frac{\Omega_g(t - t')}{2}\right) + i n_z \sin\left(\frac{\Omega_g(t - t')}{2}\right) \right] \int_0^{t'} dt'' \xi(t'') e^{-\frac{\gamma(t'' - t')}{2}} \sin\left(\frac{\Omega_e(t' - t'')}{2}\right) \sin\left(\frac{\Omega_g t''}{2}\right)
\end{aligned}$$

Appendix B: Explicit derivation of the fidelity of the coherent single photon source

Recall that $\rho_\infty = \text{Tr}_{\text{spin}}[\Psi_\infty^{(\uparrow)}\langle\Psi_\infty^{(\uparrow)}\rangle]$ and $\mathcal{F}_{\text{PNS}}(\alpha, \beta) = \langle\Psi_{\text{ideal}}|\rho_\infty|\Psi_{\text{ideal}}\rangle$. This can be neatly written by instead equipping the ideal state artificially with spin components and simply computing the fidelity of this state with $|\Psi_\infty^{(\uparrow)}\rangle\langle\Psi_\infty^{(\uparrow)}|$. We obtain

$$\begin{aligned}\mathcal{F}_{\text{PNS}}(\alpha, \beta) &= \sum_{\mu=\uparrow, \downarrow} |\alpha^* \langle 1_R, \mu, g | \Psi_\infty^{(\uparrow)} \rangle + \beta^* \langle 0, \mu, g | \Psi_\infty^{(\uparrow)} \rangle|^2 \\ &= \sum_{\mu=\uparrow, \downarrow} |\alpha^* \langle 1_L, \mu, g | \Psi_\infty^{(\downarrow)} \rangle + \beta^* \langle 0, \mu, g | \Psi_\infty^{(\downarrow)} \rangle|^2\end{aligned}\quad (\text{B1})$$

where the second equality derives from the property $f_{1_R}^{(\uparrow, \uparrow)} = (f_{1_L}^{(\downarrow, \downarrow)})^*$ and $f_{1_R}^{(\uparrow, \downarrow)} = - (f_{1_L}^{(\downarrow, \uparrow)})^*$ (see Appendix A).

Let us first write the first member of Eq. (B1) as:

$$F = |\alpha|^4 A + |\alpha|^2 |\beta|^2 B + |\beta|^4 \quad (\text{B2})$$

with

$$A = \left| \langle 1_R | \phi_R^{(\uparrow, \uparrow)} \rangle \right|^2 + \left| \langle 1_R | \phi_R^{(\uparrow, \downarrow)} \rangle \right|^2 \quad (\text{B3})$$

$$\begin{aligned}B &= \left(\cos\left(\frac{\Omega t_\infty}{2}\right) + i \cos(\theta) \sin\left(\frac{\Omega t_\infty}{2}\right) \right) \langle 1_R | \phi_R^{(\uparrow, \uparrow)} \rangle + \\ &\quad (i \cos(\phi) \sin(\theta) + \sin(\phi) \sin(\theta)) \sin\left(\frac{\Omega t_\infty}{2}\right) \langle 1_R | \phi_R^{(\uparrow, \downarrow)} \rangle + h.c.\end{aligned}\quad (\text{B4})$$

Naively it looks like there is still a t_∞ dependence, but this is not the case. We see that by writing explicitly the quantities $\langle 1_R | \phi_R^{(\uparrow, \uparrow)} \rangle$ and $\langle 1_R | \phi_R^{(\uparrow, \downarrow)} \rangle$ as a function of the two adimensional variable $x := \frac{\Omega}{2\gamma}$ and $b := \gamma t_\infty$.

$$\langle 1_R | \phi_R^{(\uparrow, \uparrow)} \rangle = \frac{\cos(xb)[1 + ix \cos(\theta)] + \sin(xb)[x - i \cos(\theta)]}{1 + x^2} \quad (\text{B5})$$

$$\langle 1_R | \phi_R^{(\uparrow, \downarrow)} \rangle = [i \sin(\theta) \cos(\phi) - \sin(\theta) \sin(\phi)] \frac{x \cos(xb) - \sin(xb)}{1 + x^2} \quad (\text{B6})$$

Entering the above expressions into A and B we get:

$$A = \frac{1}{1 + x^2}; \quad B = \frac{2}{1 + x^2}; \quad (\text{B7})$$

plugging those expressions for A and B into Eq. (B2), we obtain Eq. (13).

Appendix C: Explicit derivation of ideal working point of CZ gate

Here we show into details how the chain of inequalities required for the optimization of the CZ gate, i.e. $\gamma \gg \Gamma \gg \Omega_g \approx \Omega_e$, emerges from the explicit expressions of the coefficients A,B,C,D in Eq. (26). Let us recall that we have assumed that by the time the second photon is sent, the first photon has already been fully scattered by the QD, which means $\gamma, \Gamma \gg \Omega_g$: this also implies that in all the analytical expressions derived from the SPI wavefunction we put $e^{-\Gamma T_g/2} \rightarrow 0, e^{-\gamma T_g/2} \rightarrow 0$. In this condition, all quantities in the fidelity become functions of $\Gamma/\gamma, \Omega_{g,e}/\gamma$ and hence for ease of notation we set $\gamma = 1$ in the below expressions. Furthermore, the expressions of the overlaps $\Lambda^{(\mu, \nu)}$ greatly simplify. For instance, $\Lambda^{(\uparrow, \uparrow)}$ becomes a very simple function of the band-width ratio Γ/γ :

$$\Lambda^{(\uparrow, \uparrow)} \rightarrow \frac{-1 + \Gamma^2}{\sqrt{2}(1 + \Gamma)^2}. \quad (\text{C1})$$

Using $n_x = 1$ also gives

$$C \rightarrow \frac{\{4\Gamma^3 + 6\Gamma^4 + \Gamma(\Gamma - \Omega_g) - 3\Gamma^2\Omega_g - 3\Gamma^3\Omega_g + \Omega_g^3 + \Omega_g^2(\Omega_e^2 + \Omega_g^2) + \Gamma^2(2\Omega_e^2 + 3\Omega_g^2) + \Gamma(-\Omega_e^2\Omega_g + \Omega_g^3) + (\Gamma^2 + \Omega_g^2)[\Gamma^4 + (\Omega_e^2 - \Omega_g^2)^2 + 2\Gamma^2(\Omega_e^2 + \Omega_g^2)] + (\Gamma^2 + \Omega_g^2)[4\Gamma^3 - \Gamma^2\Omega_g - \Omega_e^2\Omega_g + \Omega_g^3 + 2\Gamma(2\Omega_e^2 + \Omega_g^2)]\}}{(1 + 2\Gamma + \Gamma^2 + (\Omega_e - \Omega_g)^2)(\Gamma^2 + \Omega_g^2)(1 + 2\Gamma + \Gamma^2 + (\Omega_e + \Omega_g)^2)} \quad (\text{C2})$$

As mentioned in the main, the condition $A = B = C = D = e^{i\delta}$ giving fidelity equal to one, can be reached at $n_x = 1$, this gives $A = 1$ and hence $\delta = 0$. The above expression for C , as expected goes to 1 in the limit $\Omega_e/\gamma \rightarrow 0$ and $\Omega_g/\gamma \rightarrow 0$:

$$C \rightarrow \frac{\Gamma^6 + 4\Gamma^5 + 6\Gamma^4 + 4\Gamma^3 + \Gamma^2}{\Gamma^2(1 + 2\Gamma + \Gamma^2)^2} = 1 \quad (\text{C3})$$

Thus we have $C \rightarrow 1$ as long as $\Omega_e \approx \Omega_g \ll \gamma, \Gamma$. Note that the relation between Γ, γ is still undetermined.

Using the result of A, C in B, D gives

$$B \rightarrow \frac{1}{2} + \frac{1}{\sqrt{2}}(-\Lambda^{(\uparrow,\uparrow)} + \Lambda^{(\downarrow,\downarrow)} + i\Lambda^{(\uparrow,\downarrow)}) \quad (\text{C4})$$

$$D \rightarrow \frac{-1}{\sqrt{2}}(i\Lambda^{(\uparrow,\downarrow)} + \Lambda^{(\downarrow,\uparrow)} + \Lambda^{(\uparrow,\uparrow)}) + (\Lambda^{(\uparrow,\uparrow)})^2 = \frac{-1}{\sqrt{2}}(i\Lambda^{(\uparrow,\downarrow)} + \Lambda^{(\downarrow,\uparrow)} - \Lambda^{(\uparrow,\uparrow)}) - \sqrt{2}\Lambda^{(\uparrow,\uparrow)} + (\Lambda^{(\uparrow,\uparrow)})^2 \quad (\text{C5})$$

Now assuming $B = 1$ gives

$$D = -\frac{1}{2} - \sqrt{2}\Lambda^{(\uparrow,\uparrow)} + (\Lambda^{(\uparrow,\uparrow)})^2 \quad (\text{C6})$$

Demanding that $D = 1$ yields

$$\Lambda^{(\uparrow,\uparrow)} = -\frac{1}{\sqrt{2}} \text{ or } \frac{3}{\sqrt{2}} \quad (\text{C7})$$

Using the explicit expression of $\Lambda^{(\uparrow,\uparrow)}$ given in Eq. (C1) we see that the only possible solution, as Γ is always positive, is $-1/\sqrt{2}$ that is attained when $\Gamma/\gamma \ll 1$. This thus fixes the last part of the chain of inequalities.
